Rate−Temperature Relationships in λ-Repressor Fragment λ_{6-85} Folding†

Wei Yuan Yang§,‡ and Martin Gruebele*,§,⊥

Center for Biophysics and Computational Biology and Departments of Chemistry and Physics, University of Illinois at Urbana-Champaign, Illinois 61801

Received May 1, 2004; Revised Manuscript Received August 3, 2004

ABSTRACT: Two classes of λ_{6-85} mutants (those richer in alanine, and those richer in glycine) have very similar slopes in an Arrhenius plot of the unfolding rates but very different temperature dependencies of the folding rates. Temperature-dependent interactions (e.g., hydrophobicity) play a large role in the initial stages of folding but not in the initial stages of unfolding of λ_{6-85}. Placement of the transition state in terms of its surface exposure and entropy shows that at least two reaction coordinates are required to describe folding of all mutants over the full temperature range. The unusual Arrhenius plots of the very fastest mutant provide an additional kinetic signature for downhill folding.

Folding rate vs temperature curves of proteins reflect the microscopic dependence of free energy landscapes on temperature. Extracting free energy information commonly first proceeds through the famous Arrhenius analysis originally introduced to interpret small molecule chemical kinetics (*1*). Unlike most small-molecule reactions, non-Arrhenius kinetics is oftentimes observed for protein folding (*2*−*6*). When the logarithm of the unfolding rate is plotted against inverse temperature, the expected straight line with negative slope is observed. In corresponding plots of the folding rate, a strong curvature or even a rate maximum is observed. A heat capacity change from hydrophobic interactions is most often held responsible (*7*−*9*). The hydrophobic effect is estimated to have a maximum strength between 0 and 100 °C (*10*−*12*). It has been proposed that maximum hydrophobicity creates a minimum folding barrier with respect to the unfolded state, thereby causing the observed maximum in the folding rate.

One can also take a more structural view of the transition state to explain the appearance of positive slopes in Arrhenius plots of refolding kinetics. For example, the folding rate of artificial and natural helical polymers decreases when the temperature is raised sufficiently: the highly structured transition state ($\Delta S^{\dagger} \ll 0$) results in a free energy barrier that grows with increasing temperature, offsetting the increased thermal excitation available for getting over the barrier (*13*, *14*). Likewise, different protein ensembles tune with temperature, denaturant, or sequence, so new folding routes can open up when they come within a few k_BT of the lowest free energy path. (*15*−*20*) Changing folding routes can cause changes in the rate−temperature dependence. In particular, the residual structure of the unfolded state is sensitive to sequence and solvent variations (*18*, *20*−*23*) and increasingly favors extended structure as the temperature is raised (*24*).

We provide new temperature- and sequence-dependent rate information for λ-repressor fragment λ_{6-85}. A salient feature of these data is the variability of the temperature dependence of the folding rates from mutant to mutant, while unfolding rates are similar for all mutants and nearly obey Arrhenius kinetics. We show that the rate−temperature relationship of λ_{6-85} can be used to probe its folding mechanism (*19*) with different λ-repressor mutants folding through very different routes. Parabolic $\ln(k_f)$ vs $1/T$ curves occur when protein folding is driven by hydrophobic collapse. Positive slopes in the folding rate Arrhenius plots of alanine-rich λ-repressor mutants occur when helix formation becomes competitive with collapse. Downhill or "type 0" folding (*15*) has been demonstrated kinetically for λD14A (*25*), a mutant with a purely negative slope. This demonstrates the complexity of protein folding landscapes, because a few point mutations can switch the dominant conformational space that λ_{6-85} travels through during folding while for other proteins large sequence variations leave the folding mechanism unaltered (*26*).

The data suggests two other interesting properties of the free energy landscape. According to our ϕ_T-value analysis, even an apparent two-state folder like λ-repressor is not fully described by a single reaction coordinate, although other evidence suggests that a small number of coordinates should suffice for λ_{6-85} (*25*). In addition, apparent cooperativity during denaturation can also arise from structural reorganization within the unfolded ensemble of λ_{6-85}, not just from two-state folding over a barrier. This has been proposed and observed elsewhere also (*27*−*31*).

EXPERIMENTAL PROCEDURES

λ-Repressor Expression and Purification. The λ-repressor N-terminal (*32*, *33*) domain gene (residues 6−85, obtained from T. Oas) was inserted into the PET-15b vector (Novagen) between the *Nde*I and *Bam*HI cutting sites, allowing histidine−nickel binding-based purification. Point mutations were made with the QuickChange site-directed mutagenesis kit

† This work was supported by the National Science Foundation Grant MCB 0316925.

* Corresponding author. Tel: (217) 333-1624. Fax: (217) 244-3186. E-mail: gruebele@scs.uiuc.edu.

§ Center for Biophysics and Computational Biology.

‡ Current address: Department of Chemistry and Chemical Biology, Harvard University, Cambridge, MA 02138.

⊥ Departments of Chemistry and Physics.

10.1021/bi049113b CCC: $27.50
Published on Web 09/23/2004

Table 1: λ-Repressor Mutants Used[a]

name	mutations	m (kT_o/M)	C_m (M)	T_m (°C)	log(k[T_m]) (k in μs^{-1})
λD14A	D14A, Y22W, Q33Y, G46A, G48A	3.3	2.76	73.5	−0.70
λA49G	D14A, Y22W, Q33Y, A37G, G46A, G48A, A49G			62.5	−1.25
λQ33Y	Y22W, Q33Y, G46A, G48A	3.7	3.27	71.0	−1.20
λA37G	Y22W, Q33Y, A37G	3.1	1.62	59.5	−1.35
λS45A	Y22W, Q33Y, G46A, S45A, G48A	3.7	3.42	69.5	−1.10
λS79A	Y22W, Q33Y, G46A, S45A, G48A, S79A	3.6	3.25	70.5	−1.15
λWT	Y22W	3.6	2.04	61.0	−1.25
λG46A	Y22W, G46A, G48A	3.7	2.78	67.5	−1.30
λsQ33Y	Y22W, Q33Y			61.5	−1.30
λsA37G	Y22W, A37G	3.1	1.62	54.5	−1.35
λsA63V	Y22W, A63V	3.3	2.17	60.0	−1.40
λsG46A	Y22W, A37G, G46A, G48A, A49G			56.0	−1.40
λsA49G	Y22W, A37G, A49G	2.8	1.10	47.0	−1.60
λsA81G	Y22W, Q33Y, A37G, A49G, A81G	2.8	1.20	47.5	−1.40
λnQ33Y	Y22W, Q33Y, A37G, A49G	3.1	1.61	54.5	
λM42G	Y22W, Q33Y, M42G, S45A, G46A, G48A, S79A	3.4	2.14	59.0	−1.40

[a] Thermodynamic parameters m and C_m at 20 °C were obtained using GuHCl as the denaturant and eq 3 in the form $\Delta G = m(C - C_m)$. C_m is the denaturant concentration when half of the proteins are unfolded; therefore, the stability of each mutant without the presence of GuHCl is mC_m. T_m is the thermal denaturation midpoint in absence of GuHCl to the nearest 0.5 °C, and k is the observed rate at the midpoint.

(Stratagene). Proteins were expressed in Rosetta(DE3) pLysS (Novagen) cells with the media 20 g/L tryptone, 10 g/L yeast-extract, 5 g/L NaCl, 200 mg/L ampicilin, 35 mg/L chloramphenicol, and 4 g/L glucose at pH 7.4. Expression was induced with 2 mM isopropyl-β-D-thiogalactopyranoside (IPTG), and cells were grown at 28 °C. Harvested cells were lysed by passing them through a French press twice at >12 000 psi, and λ-repressor was normally found in the soluble fraction. Purification on a Ni−NTA column (Qiagen) with imidazole as the eluting reagent was followed by a size-exculsion column, such as a Sephacryl S-200 HR column (Amershan Pharmacia) at pH 8, 20 mM Tris, and 500 mM NaCl. Histidine tags were removed with thrombin (Novagen), using 1 unit of thrombin per milligram of λ-repressor. The cleavage time was 16 h at room temperature. Histidine tags were than separated from the protein solution by dialysis or with the Ni−NTA column. Pure proteins were dialyzed extensively against deionized water and lyophilized for storage at −20 °C. Low-resolution electrospray-ionization mass spectrometry was used to confirm the desired mutations. Expression levels of proteins were closely related to the mutant stabilities.

λ-Repressor Mutants. The abbreviated names for the λ-repressor mutants used, together with a full description of the mutations, are listed in Table 1. Mutations include glycine to alanine at positions 46 and 48, used previously used by Oas to stabilize the third helix of λ-repressor and greatly increase the folding rate (*20*), alanine to glycine mutations at position 37, 49 (near the start and end of the third helix), and 81 (fifth helix), three positions with water-exposed side chains (which have been shown to have minimal effect on λ-repressor folding), serine to alanine mutations at position 45 and 79 further stabilize the least-stable helices (3 and 5, as indicated by the percentage helical content calculated through AGADIR) (*34*), an alanine to valine mutation at position 63 to enlarge the side chain pointing into the hydrophobic core, allowing for a easier hydrophobic collapse, Asp14Ala and Gln33Tyr mutations, known to speed up folding (Oas, private communication, and refs *25* and *35*), and a methionine to glycine mutation to remove a set of unfavorable dihedral angles for the methionine in loop 2.

λ-Repressor Measurements. Protein concentrations in all measurements were estimated using 280 nm absorption of the protein solution assuming the extinction coefficient of 5600 cm^{-1} M^{-1} for trytophans and 1300 cm^{-1} M^{-1} for tyrosines. Circular dichroism measurements were carried out on a JASCO J-715 equipped with a Peltier temperature controller. Temperature-jump-induced relaxation kinetics were done with a 10 ns CH_4 Raman-shifted Nd:YAG water heating pulse (1540 nm) with T-jump sizes ranging between 10 and 12 °C. Folding was probed by a 14 ns spaced pulse train of 280 nm light, exciting the tryptophan in λ-repressors. Changes in tryptophan fluorescence emission lifetimes were used to track the protein folding kinetics (*36*).

The folding and unfolding rates were obtained by fitting the T-jump-induced relaxation rate coefficients, k, at each temperature; k and the equilibrium constant $K(T)$ were used to compute the folding and unfolding rate coefficients. $K(T)$ was calculated from $\Delta G(T)$, obtained from protein thermal denaturation curves monitored by circular dichroism at 222 nm. We approximated the protein stabilities by quadratic functions of the temperature, $\Delta G = \Delta G_0 + \Delta G_1(T - T_m) + \Delta G_2(T - T_m)^2$. The rates were then obtained as

$$k_f(T) = k(T)K(T)/(1 + K(T)) \quad (1a)$$

$$k_u(T) = k(T)/(1 + K(T)) \quad (1b)$$

Very fast-folding mutants (λD14A, λQ33Y) show a very fast molecular time scale in addition to the activated folding kinetics, caused by diffusive downhill folding on a rough free energy surface (*35*, *37*). For these, we used the long-time exponential fit to obtain an approximate k (*25*).

ϕ_T Analysis. ϕ_T analysis uses temperature derivatives of $\Delta G(T)$ to find the relative placement of the transition state along an entropic reaction coordinate defined as (*6*, *19*)

$$\Phi_T = \frac{\partial \Delta G^{\dagger}/\partial T}{\partial \Delta G/\partial T} = \frac{\Delta S^{\dagger}}{\Delta S} \quad (2)$$

$\Phi_T \approx 1$ when the transition state ensemble lies near the native state along this reaction coordinate. $\Phi_T < 1$ indicates relative motion of the transition state ensemble toward the unfolded

Table 2: Fitted Parameters for the Native State Stability and Folding Activation Energy of the Mutants for Which Θ_T Was Calculated[a]

name	T_m (°C)	ΔG_0[b]	ΔG_1	ΔG_2	$\Delta G_0^\dagger$	$\Delta G_1^\dagger$	$\Delta G_2^\dagger$	R·slope
λWT	61.0	0	0.68	0.0046	7.8	−0.020	0.0030	−35
λQ33Y	71.0	0	0.72	0.0025	9.0	0.273	0.0013	−41
λG46A	67.5	0	0.72	0.0038	9.0	0.300	0.0042	−37
λsA37G	54.5	0.3	0.62	0.0073	9.4	0.144	0.0099	−36
λsA63V	56.0	−0.1	0.58	0.0039	9.2	0.096	0.0095	−36

[a] All coefficients are in kJ/(mol K^n) units, n being the subscript of the coefficient. Slope is the slope of the plots in Figure 4 at T_m after removing the viscosity temperature dependence. [b] These coefficients are nominally zero if T_m is used as the reference temperature but are shown where rounding of T_m to the nearest 0.5 °C (the estimated measurement uncertainty) caused a value ≥0.1 kJ/mol in the fit.

state; in absolute structural terms, this may be caused by a less nativelike transition state, a more nativelike unfolded ensemble, or both (*38*). To obtain ϕ_T, the folding activation free energies were approximated by quadratic functions in T ($\Delta G_u^\dagger(T) = \Delta G_0^\dagger + \Delta G_1^\dagger(T - T_m) + \Delta G_2^\dagger(T - T_m)^2$), where T_m is the heat denaturation transition midpoint. The coefficients were fitted to the observed folding rate by applying Kramers' theory, $k_f = \nu^\dagger[\eta(T_m)/\eta(T)]\ e^{-\Delta G_f^\dagger/(RT)}$. We used $\nu^\dagger(T_m) \approx (1.5\ \mu s)^{-1}$ (*35*) and took into account the temperature dependence of the water viscosity. The fitted parameters for some of the mutants discussed in more detail are listed in Table 2.

RESULTS

Stability−Cooperativity Correlation. *m*-values measure folding cooperativites obtained from denaturant titrations, assuming a linear free-energy relationship (*39*):

$$\Delta G \approx \Delta G_{20} + \left.\frac{\partial \Delta G}{\partial C}\right|_{C=0} C = \Delta G_{20} + mC \qquad (3)$$

where C is the denaturant concentration and ΔG_{20} is the folding free energy at 20 °C. The folding cooperativity of λ-repressor mutants studied by GuHCl[1] titration is correlated with the folding stability of each variant (Figure 1). The correlation is $m = 2.6 + 0.091\Delta G_{20}$ in the units of Tables 1 and 2. Thus the free energy in eq 3 depends to a good approximation only on a single parameter for all the mutants: $\Delta G \approx m(C + 11) - 28$. The thermal unfolding midpoint temperatures, T_m, show a similar correlation with m (Figure 1), as do the thermal titration cooperativities,

$$\left.\frac{\partial \Delta G}{\partial T}\right|_{T=T_m} = \Delta G_1 \qquad (4)$$

(Table 2). λD14A is the notable exception to the rule: addition of the D14A mutation decreases C_m and m but increases T_m. The mutant undergoes more facile chaotropic denaturation yet less facile thermal denaturation.

Unfolded and Folded λ_{6-85} CD Baselines. In our thermal denaturation experiments monitored by CD, we found that the linear baseline slopes for the unfolded states are much larger in the alanine-rich variants of λ_{6-85}. The ordering follows precisely the numbers of alanines in the mutants:

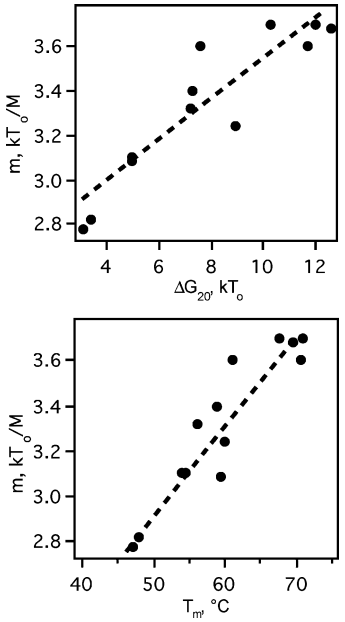

FIGURE 1: The top graph shows the correlation between GuHCl *m*-value and ΔG in λ_{6-85} (see eq 3). A similar correlation is obtained between ΔG and thermal cooperativities from Table 2. The bottom graph shows the correlation between *m*-value and melting temperature. λD14A tends to violate such correlations (Table 1).

the unfolded states of alanine-rich mutants gain secondary structure more easily when the temperature is lowered. For example, we compare three mutants with very different alanine contents (Figure 2). The most alanine-rich mutant, λG46A, has an unfolded baseline slope of 0.061 mdeg °C^{-1} μM^{-1}, whereas it is 0.042 mdeg °C^{-1} μM^{-1} for λWT and 0.027 mdeg °C^{-1} μM^{-1} for λsA49G. On the other hand, the folded baseline slope is the smallest in the alanine-rich mutants because alanines provide better stability and packing to the native fold. λD14A actually has a negative folded baseline slope.

Folding Rate Temperature Dependence. Like many other proteins (*2*), λ-repressors exhibit non-Arrhenius folding behavior. The curvatures of different mutants vary widely with higher folding rate associated with more stable variants. Figure 3 shows the measured activated relaxation rate constants (not the additional fast molecular phase observed for the fastest mutants (*35*)). Our measurements can be grouped roughly into mutants containing G46A/G48A mutations and ones that do not have the two engineered alanines or additional glycines. The set of mutants containing more alanines vs glycines exhibit positive slopes in ln k vs $1/T$ plots across their folding transitions, except for λD14A. The group with more glycines vs alanines shows parabolic behavior.

Comparison with the denaturant extrapolations from ref *20* (Chevron plots) shows that our predicted folding rates at 37 °C are always equally fast or faster than the extrapolated rates from NMR line width measurements. The fastest observed activated rate coefficient (~9 μs for λD14A at 353 K) corresponds to a barrier of 2.2 kT (using the measured prefactor from ref *35*). A value of 2.2 kT barely lies within the range where Kramers' model can be applied. The fastest folding rate extrapolated from both NMR and *T*-jump experiments is (4 μs)$^{-1}$ for λQ33Y at 320 K, well outside the Kramers' regime.

[1] Abbreviations: GuHCl, guanidinium hydrochloride; WT, wild-type; CD, circular dichroism.

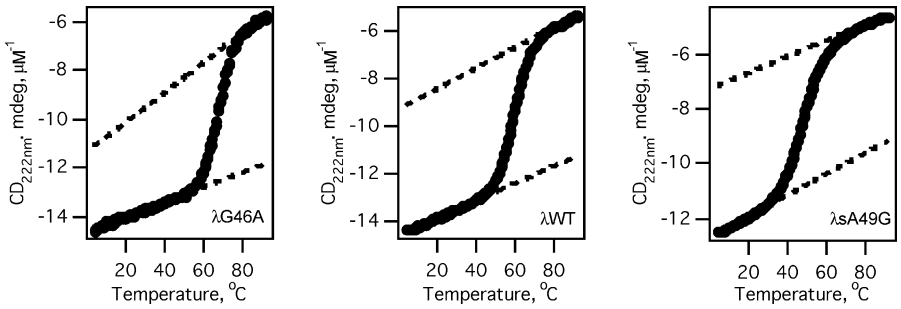

FIGURE 2: Slopes of the unfolded baseline become less steep as alanines are mutated into glycines. λG46A has two extra alanines compared to λWT and four extra alanines when compared to λsA49G.

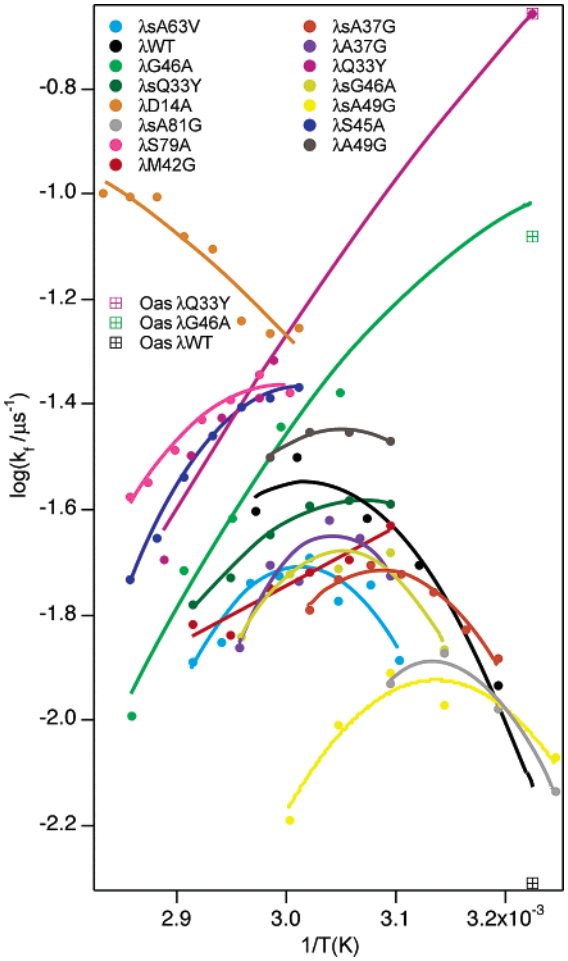

FIGURE 3: Folding rates with quadratic free energy fits of different mutants obtained from our *T*-jump studies and extrapolated rates (squares) using denaturants by Oas and co-workers. Different mutants display very different curvatures on a ln *k* vs 1/*T* plot.

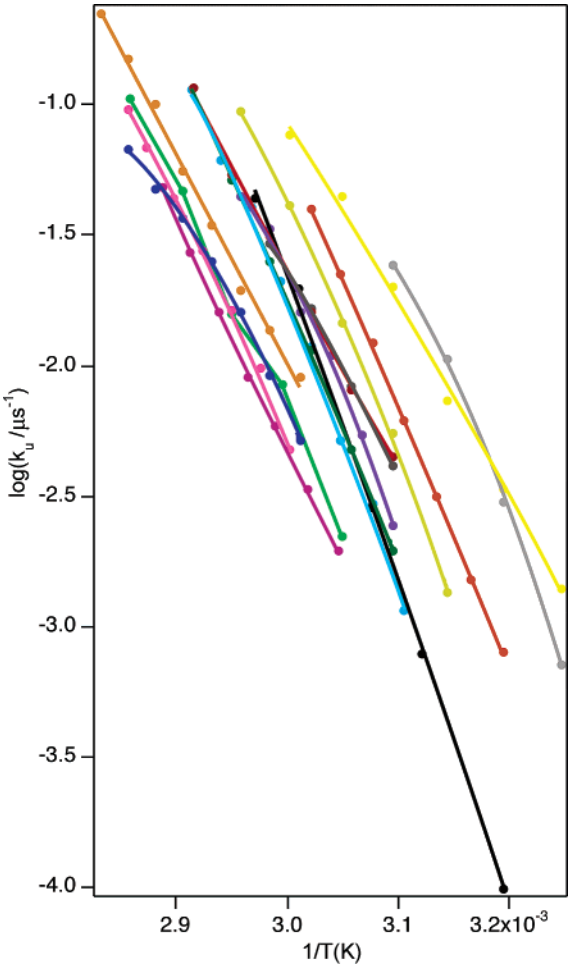

FIGURE 4: Regardless of mutations done to λ-repressor, the observed unfolding rates for different mutants show up as parallel straight lines on a ln *k* vs 1/*T* plot (color codes as in Figure 3).

Unfolding Rate Temperature Dependence. The unfolding rates of different mutants are well-approximated by a set of nearly parallel straight lines with negative slopes on a ln *k* vs 1/*T* plot (Table 2, Figure 4). At the denaturation midpoint temperature, T_m, where bias toward the denatured and native state has been removed ($\Delta G = 0$), we find that $\log(k \cdot \mu s) = \log(2k_u \cdot \mu s)$ is nearly constant: the standard deviation is ± 0.2, and only λD14A is an outlier (Table 1). However, stable mutants unfold more slowly than less stable mutants at a given constant temperature (Figure 4).

Assuming a common prefactor for all mutants of λ_{6-85} ($k_m \approx [1.5\ \mu s \cdot \eta(25\ ^\circ C)/\eta(T)]^{-1}$ (*35*)), the parallel straight lines with an offset require that $\Delta G_u^\dagger$ be approximately linear in temperature and expressed as $\Delta G_u^\dagger = \Delta G_{u0}^\dagger + \Delta G_{u1}^\dagger(T - T_m)$, where T_m are the thermal denaturation midpoints for different mutants listed in Table 1. Similarity between all the negative slopes (e.g., Table 2) indicates that $\Delta G_{u0}^\dagger - \Delta G_{u1}^\dagger T_m$ stays approximately constant across all λ_{6-85} variants. Independently of that, the small spread of rates at T_m indicates that $\Delta G_u^\dagger(T_m) = \Delta G_f^\dagger(T_m)$ stays roughly constant across all mutants (D14A excepted), leaving only a weak correlation with stability ΔG_{20} at T_m.

From Kramers' rate law, $\ln(k_u/\nu_u^\dagger) = -\Delta G_u^\dagger/(RT)$, $\Delta G_u^\dagger$ for different variants ranges from 2.1 to 5.8 kT at 325 K. The fastest unfolders lie barely at the edge of applicability of Kramers' law.

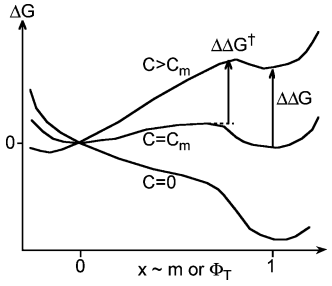

FIGURE 5: Free energy as a function of a relative reaction coordinate such as m or Φ_T. Two points important for the discussion are illustrated: first, the free energy of a late transition state and of the folded state respond similarly to perturbations, so k_u obeys Arrhenius kinetics; second, perturbations (GuHCl, T) that raise the native free energy also raise the free energy of the activated region, so a barrier develops even for proteins that fold downhill under ideal conditions. Such a barrier will lie late along the reaction coordinate.

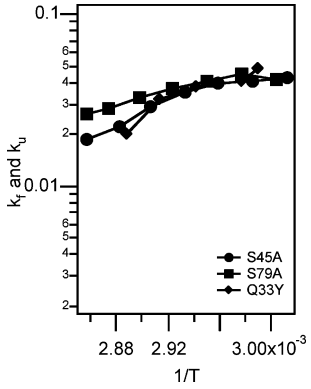

FIGURE 6: Comparison of three G46A/G48A mutants. At low temperatures, the folding rates are similar. At higher temperatures, mutants with higher alanine contents show higher folding rates.

DISCUSSION

Two-State Assumption. Several of the λ_{6-85} mutants discussed here fold very rapidly and show a very fast phase k_m preceding the activated kinetics (*35*). Based on a large body of data (*25*), we assigned this phase to diffusion among local minima of the rough free energy landscape in the absence of a barrier ("downhill folding").

This observation does not necessarily preclude a thermodynamic two-state analysis of fast-folding mutants when temperature or GuHCl denaturation is used. Figure 5 illustrates this with a simplified one-dimensional reaction coordinate for GuHCl titration. When all free energies are referenced to the unfolded state, the m-value varies from 0 to m_{native} along the reaction coordinate. Therefore $m^\dagger \approx m_{native}$ if the transition state lies near the native state. When a protein is GuHCl-titrated, a barrier will therefore develop at the transition midpoint, even if the protein or peptide is sufficiently stable to fold downhill under conditions maximally favorable for forming the native state (*40*). For this apparent two-state transition, we can invoke $K = k_f/k_u$ to relate forward and backward rate constants, as was done in Figures 3 and 4 to compute them from the observed activated relaxation time.

The two-state approximation during temperature or chaotropic unfolding breaks down only for strong downhill folders, the barrier of which is below a few kilotesla even at the denaturation midpoint. λD14A is in this limit (*25*). Indeed, λD14A is the exception to the rule in almost all the two-state analyses summarized in the results section. Ironically, the fact that λD14A has a negative slope in both the folding and unfolding Arrhenius plots (considered to be normal behavior for small molecule unimolecular reactions) can be explained as a new kinetic signature of downhill folding: without an entropic barrier that increases with temperature, there will be no rate turn-around as the k_f and k_u time scales merge with the k_m time scale during downhill folding. The merging of the folding and unfolding rate−temperature relationships also means a loss of apparent cooperativity in the thermal denaturation curves, as observed for λD14A (*25*).

Non-Arrhenius Folding Rates: Hydrophobicity and Helix Stability. The strength of the hydrophobic effect is approximately parabolic with a maximum between 0 and 100 °C. The folding rates of slower glycine-rich mutants show a parabolic turnover because their activation free energies have large quadratic coefficients $\Delta G_2^\dagger$. They fold by a hydrophobic collapse mechanism dominated by a heat capacity change (*41*). Collapse proceeds most efficiently when hydrophobic interactions are maximized, and this is where slow mutants fold most rapidly. A parabolic rate−T curve has been observed by Muñoz and co-workers for the collapse of an unfolded miniprotein (*42*).

Among alanine-rich mutants, the hydrophobic effect is masked by an even larger temperature dependence of the secondary structure content. Helices are stabilized at lower temperature, counteracting the decrease in hydrophobicity that ultimately causes cold-denaturation of the less stable mutants. As a result, the folding rate continues to increase as the temperature is lowered (Figure 3), instead of turning over. The connection with secondary structure becomes clear in Figure 2. The alanine-rich mutants show considerably more structure (larger CD_{222}) in the folded and unfolded states, and the secondary structure content of their heat-denatured state increases more rapidly when the denatured state is cooled (steeper unfolded baselines in Figure 2). As a result, alanine-rich mutants approach framework-like folding at low temperature (*43*).

This argument can be further strengthened by looking more closely at G46A/G48A mutants that contain additional alanine mutations (Figure 6). The folding rates of the three mutants λQ33Y, λS45A, and λS79A all increase when the temperature is lowered. The rate of λS79A, which contains the most alanines, increases less rapidly than the other two because λS79A already has more helical structure even at high temperature. The rate follows a nice progression of λS79A > λS45A > λQ33Y at higher temperatures, in accordance with the number of helix-enhancing mutations.

Our observations are consistent with Oas' measurements on λ-repressors. In his rate−denaturant studies at 37 °C, he finds the transition state for G46A/G48A mutants to be highly water-accessible: $\alpha^\dagger = m^\dagger/m_{native} = 0.04-0.2$ ($\alpha^\dagger$ is 0 when the transition structure is as solvated as the unfolded structures, and $\alpha^\dagger$ is 1 when the transition structure is desolvated like native state) (*39*, *44*, *45*). In the wild-yype protein, the transition state is less surface-exposed ($\alpha^\dagger = 0.6$) (*20*, *46*). This corresponds well with two different folding mechanisms. Very stable secondary structure allows the

transition state to form earlier without extensive desolvation, while less stable secondary structure requires more water to be expelled so contacts can be made and the transition state can be reached.

Non-Arrhenius Folding Rates: Other Contributions. The parabolic rate−temperature relationships for the slow-folding mutants have slightly different curvatures and maximize k_f at different temperatures, T_{max}. Even after any unfolded/native bias is removed by comparing $T_{max} - T_m$, a small spread (standard deviation ±4 °C) remains. There are secondary competing mechanisms underlying their folding, beyond the temperature dependence of hydrophobicity and secondary structure. The residual rms fluctuation of the free energy surface for λ_{6-85} has been determined at $G_{RMS} \approx 0.8$ kT by fitting fast folding data with a Langevin dynamics model on a nearly downhill free energy surface (*25*). The data presented here is not sufficient to indicate whether such fluctuations can account for the differences seen in Figure 4.

Similarity of Transition and Native States. Like the folding activation energies, the folding free energies have large quadratic terms, leading to a temperature of maximum stability from which the protein cold or heat denatures. In the thermodynamic cycle relating ΔG, $\Delta G_u^\dagger$, and $\Delta G_f^\dagger$, these terms nearly cancel. Thus $\Delta G_u^\dagger \approx \Delta G_{u0}^\dagger + \Delta G_{u1}^\dagger(T - T_m)$ is nearly linear in temperature, and the unfolding Arrhenius plots are nearly linear. The small size of the quadratic term implies that temperature-sensitive hydrophobic interactions on a small (<10 Å) length scale have already been made when the transition state has been reached, leaving only weakly temperature-dependent interactions, such as van der Waals packing, for the last step of folding. In addition, desolvation of large hydrophobic surfaces, which may be less temperature-dependent than small-scale solvation, could contribute to the last step of folding (*47*). This criterion (but not necessarily others, see next subsection) is in accord with the view that the transition states for folding are expanded versions of the native state (*46*, *48*), retaining many of the native secondary structures with the hydrophobic core incompletely dried.

But the Arrhenius plots in Figure 4 are not just linear: the Arrhenius slopes are very similar for all mutants (Table 2), and when referenced to T_m, the spread in relaxation rates is small among mutants (Table 1; except for λD14A). This, together with the near-linearity of $\Delta G_u^\dagger(T)$, implies that $\Delta H_u^\dagger = \Delta G_{u0}^\dagger - T_m\Delta G_{u1}^\dagger$ and $\Delta G_{u0}^\dagger$ are both insensitive to mutation.

We rationalize these two observations in terms of the flexible core repacking upon "conservative" small mutations. Core repacking upon glycine to alanine mutatation leaves $\Delta H_u^\dagger$ essentially independent of mutation because the van der Waals surfaces to be separated and solvated during initial unfolding do not change much from protein to protein. Even for nearly downhill folders (λD14A, λQ33Y), this constant slope holds: their unfolding free energy barrier may be close to zero, but not their $\Delta H_u^\dagger$. This highlights the fact that $\Delta S_u^\dagger \approx -\Delta G_{u1}^\dagger$ is not conserved: glycine to alanine mutations are not conservative with regard to entropy. Glycine increases the allowable motions once the core has been partially broken and solvated; the resulting higher entropy leads to lower unfolding barriers of glycine-rich mutants at a given temperature and hence faster unfolding rates (Figure 4). At the same time, the lower stability of glycine-rich mutants decreases T_m, so $\Delta S_u^\dagger$ and T_m are anticorrelated, leaving the combination $\Delta G_{u0}^\dagger = \Delta H_u^\dagger + T_m\Delta G_{u1}^\dagger$ also mutation-insensitive.

It is worth noting that alanine to glycine mutations are conservative only from the point of view of early unfolding, while the backbone structure remains confined. Glycines can cause major changes in unfolded state flexibility and even changes in the early reaction coordinates followed by protein ensembles during folding, as discussed next.

ϕ_T vs $\alpha^\dagger$ Analysis: A One-Dimensional Reaction Coordinate Is Not Enough. $\alpha^\dagger$ and Φ_T provide two different reaction coordinates based on solvent exposure and residual entropy of the transition state. Since two different folding routes are taken by alanine-rich and alanine-poor mutants, one may ask whether $\alpha^\dagger$ and Φ_T can distinguish among them.

For the alanine-rich mutants λQ33Y and λG46A, we find transition states with large and temperature-insensitive Φ_T (Figure 7). On the other hand, the alanine-poor mutants λWT, λsA37G, and λsG46A have low ϕ_T values that are very sensitive to increasing temperature.

At 37 °C, we encounter an apparent dilemma when comparing these results with $\alpha^\dagger$. Now the alanine-rich mutants have a small value of $\alpha^\dagger$ (λQ33Y $\alpha^\dagger = 0.04$, λG46A $\alpha^\dagger = 0.2$) (*20*, and Oas, private communication), while the alanine-poor mutants have a more nativelike transition state (λWT has $\alpha^\dagger = 0.6$). The trend is reversed compared to Φ_T extrapolated to 37 °C (Figure 7), demonstrating that a single reaction coordinate (such as $\alpha^\dagger$ or Φ_T alone) cannot simultaneously describe the fast- and slow-folding variants of λ_{6-85}. These results can be reconciled easily on a higher-dimensional free energy surface, as illustrated in Figure 8. The ordering of three local minima depends on the choice of reaction coordinate (the direction ADB is reversed to ABD) in one dimension, whereas this issue does not arise with the more complete two-dimensional description.

We recently reported a different constraint on the number of reaction coordinates needed to describe fast-folding λ_{6-85} mutants. Observation of a very fast diffusion-controlled "molecular phase", resulting from downhill folding limited only by residual roughness of the free energy surface, showed that the diffusion could be described by a stretched exponential $\exp[-(kt)^\beta]$ with β in the range 0.7−1 (*25*, *50*). It has been shown that diffusion on a one-dimensional rough free energy surface still yields single-exponential kinetics (*51*), while multidimensional surfaces are more prone to stretched kinetics or observable-dependent kinetics (a subset of trajectories is prone to wander along unproductive coordinates) (*50*, *52*−*55*). Thus $\beta \approx 0.7$ implies a low dimensionality, while present reaction coordinate analysis implies $D \geq 2$ for a full description of the process. The analysis of very fast folding combined with reaction coordinate analysis could provide firm lower and upper experimental bounds on the number of modes required for a full description of folding. So far, the results are consistent with theoretical analyses by principal coordinate decomposition, molecular dynamics, or potential surface graphs, indicating a small number of coordinates, but more than 1, is required for a complete low-resolution description of folding (*17*, *56*, *57*).

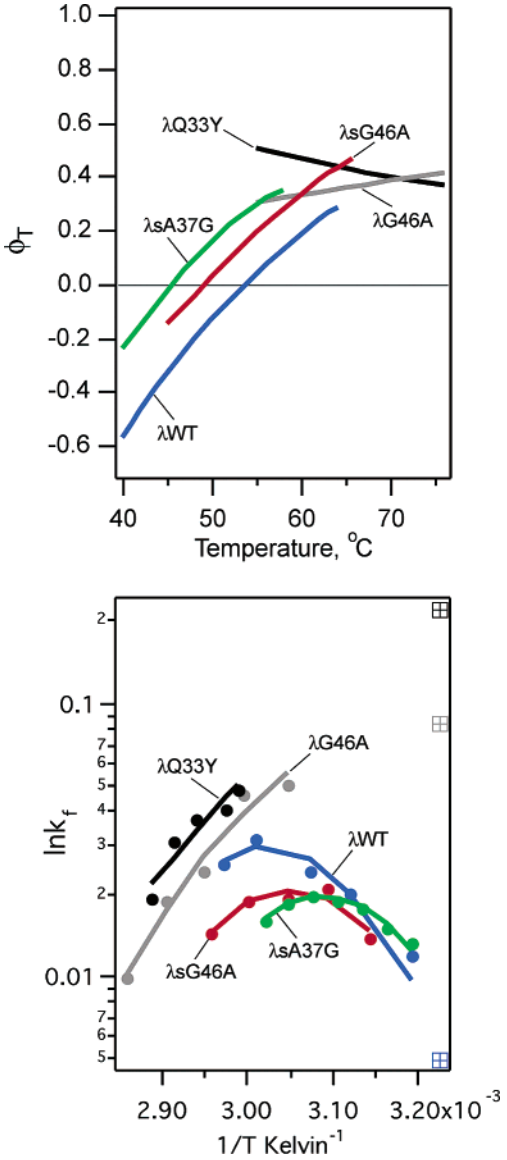

FIGURE 7: The left plot shows ϕ_T values for five representative λ-repressor mutants. The black and gray lines are alanine-rich mutants, showing higher ϕ_T value at low temperatures than the alanine-poor mutants. The right plot shows fitted folding rates assuming a parabolic activation folding free energy as a function of temperature.

Conclusions. Folding of λ_{6-85} proceeds through at least two different routes. A few point mutations or 20−30 °C temperature changes are sufficient to effect a switch, so barriers on the free energy surface limiting access to these routes cannot differ by more than a few kilotesla (*19*). Different experimental reaction coordinates contribute differently to these routes and can be used to set lower limits on the number of reaction coordinates required to describe folding. For folding glycine-rich λ_{6-85}, the folding rate is controlled by hydrophobic collapse, whereas for alanine-rich mutants, the rate−temperature behavior is dominated by residual secondary structure. The unfolding free energy of activation shows "universal" characteristics independent of mutant, with the exception of λD14A, which also differs from other mutants in all other aspects of a two-state analysis. The temperature tuning of its apparent folding and unfolding rate coefficients is a new criterion for downhill folding.

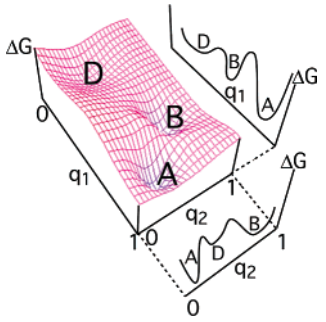

FIGURE 8: Reaction coordinates with opposite tendencies in a one-dimensional free energy plot can be reconciled in two dimensions. The denatured state D and two other local free energy minima A and B can interconvert using two coordinates q_1 and q_2: in 1-D, minima A and B are ordered differently using q_1 and q_2; in 2-D this is seen to be an artifact, and both coordinates are required to fully describe the possible routes (D−A, A−B, and B−D).

REFERENCES

1. Arrhenius, S. (1889) On the Reaction Velocity of the Inversion of Cane Sugar by Acids, *Z. Phys. Chem. 4*, 226−248.
2. Jackson, S. E., and Fersht, A. R. (1991) Folding of Chymotrypsin inhibitor-2. II. Influence of protein isomerization on the folding kinetics and thermodynamic characterization of the transition-state of folding, *Biochemistry 30*, 10436−10443.
3. Oliveberg, M., Tan, Y. J., and Fersht, A. R. (1995) Negative activation enthalpies in the kinetics of protein folding, *Proc. Natl. Acad. Sci. U.S.A. 92*, 8926−8929.
4. Scalley, M. L., and Baker, D. (1997) Protein folding kinetics exhibit an Arrhenius temperature dependence when corrected for the temperature dependence of protein stability, *Proc. Natl. Acad. Sci. U.S.A. 94*, 10636−10640.
5. Schindler, T., and Schmid, F. X. (1996) Thermodynamic properties of an extremely rapid protein folding reaction, *Biochemistry 35*, 16833−16842.
6. Crane, J. C., Koepf, E. K., Kelly, J. W., and Gruebele, M. (2000) Mapping the transition state of the WW domain beta sheet, *J. Mol. Biol. 298*, 283−292.
7. Sharp, K. A., Nicholls, A., Friedman, R., and Honig, B. (1991) Extracting Hydrophobic Free Energies from Experimental Data: Relationship to Protein Folding and Theoretical Models, *Biochemistry 30*, 9686−9697.
8. Collet, O., and Chipot, C. (2003) Protein folding in the landscape perspective: chevron plots and non-Arrhenius kinetics, *J. Am. Chem. Soc. 125*, 6573−6580.
9. Chan, H. S., and Dill, K. A. (1998) Protein folding in the landscape perspective: Chevron plots and non-Arrhenius kinetics, *Proteins 30*, 2−33.
10. Pollack, G. L. (1991) Why gases dissolve in liquids, *Science 251*, 1323−1330.
11. Hummer, G., Garde, S., Garcia, A. E., and Pratt, L. R. (2000) New perspectives on hydrophic effects, *Chem. Phys. 258*, 349−370.
12. Garde, S., Garcia, A. E., Pratt, L. R., and Hummer, G. (1999) Temperature dependence of the solubility of nonpolar gases in water, *Biophys. Chem. 78*, 21−32.
13. Thompson, P. A., Eaton, W. A., and Hofrichter, J. (1997) Laser temperature jump study of the helix ⇌ coil kinetics of an alanine peptide interpreted with a 'kinetic zipper' model, *Biochemistry 36*, 9200−9210.
14. Yang, W., Prince, R., Sabelko, J., Moore, J. S., and Gruebele, M. (2000) Transition from exponential to nonexponential kinetics during formation of an artificial helix, *J. Am. Chem. Soc. 122*, 3248−3249.
15. Onuchic, J. N., Wolynes, P. G., Luthey-Schulten, Z., and Socci, N. D. (1995) Toward an Outline of the Topography of a Realistic Protein Folding Funnel, *Proc. Natl. Acad. Sci. U.S.A. 92*, 3626−3630.
16. Bieri, O., Wildegger, G., Bachmann, A., Wagner, C., and Kiefhaber, T. (1999) A salt-induced kinetic intermediate is on a new parallel pathway of lysozyme folding, *Biochemistry 38*, 12460−12470.

17. Shea, J., and Brooks, C. L. (2001) From folding theories to folding proteins: a review and assessment of simulation studies of protein folding and unfolding, *Annu. Rev. Phys. Chem 52*, 499−535.
18. Arai, M., Kataoka, M., Kuwajima, K., Matthews, C. R., and Iwakura, M. (2003) Effects of the difference in the unfolded-state ensemble on the folding of *Escherichia coli* dihydrofolate reductase, *J. Mol. Biol. 329*, 779−791.
19. Jäger, M., Nguyen, H., Crane, J., Kelly, J., and Gruebele, M. (2001) The folding mechanism of a β-sheet: The WW domain, *J. Mol. Biol. 311*, 373−393.
20. Burton, R. E., Huang, G. S., Daugherty, M. A., Calderone, T. L., and Oas, T. G. (1997) The energy landscape of a fast-folding protein mapped by Ala → Gly Substitutions, *Nat. Struct. Biol. 4*, 305−310.
21. Sanchez, I. E., and Kiefhaber, T. (2003) Hammond behavior versus ground-state effects in protein folding: Evidence for narrow free energy barriers and residual structure in unfolded states, *J. Mol. Biol. 327*, 867−884.
22. Plaxco, K. W., and Gross, M. (2001) Unfolded, yes, but random? Never!, *Nat. Struct. Biol. 8*, 659−660.
23. Dyson, H. J., and Wright, P. E. (1998) Equilibrium NMR Studies of Unfolded and Partially Folded Proteins, *Nat. Struct. Biol. 5*, 499−503.
24. Yang, W., Larios, E., and Gruebele, M. (2003) On the extended beta-conformational propensity of polypeptides at high temperature, *J. Am. Chem. Soc. 125*, 16220−16227.
25. Yang, W., and Gruebele, M. (2004) Folding lambda repressor at its speed limit, *Biophys. J. 87*, 596−608.
26. Wallace, L. A., and Matthews, C. R. (2002) Highly divergent dihydrofolate reductases conserve complex folding mechanisms, *J. Mol. Biol. 315*, 193−211.
27. Onuchic, J. N., Luthey-Schulten, Z., and Wolynes, P. G. (1997) Theory of Protein Folding: The Energy Landscape Perspective, *Annu. Rev. Phys. Chem. 48*, 545−600.
28. Sabelko, J., Ervin, J., and Gruebele, M. (1999) Observation of strange kinetics in protein folding, *Proc. Natl. Acad. Sci. U.S.A. 96*, 6031−6036.
29. Parker, M. J., and Marqusee, S. (1999) The cooperativity of burst phase reactions explored, *J. Mol. Biol. 293*, 1195−1210.
30. Muñoz, V. (2002) Thermodynamics and kinetics of downhill protein folding investigated with a simple statistical mechanical model, *Int. J. Quantum Chem. 90*, 1522−1528.
31. Osváth, S., Sabelko, J., and Gruebele, M. (2003) Tuning the heterogeneous early folding dynamics of phosphoglycerate kinase, *J. Mol. Biol. 333*, 187−199.
32. Hecht, M. H., Sturtevant, J. M., and Sauer, R. T. (1984) Effect of single amino acid replacements on the thermal stability of the NH2 terminal domain of phage lambda repressor, *Proc. Natl. Acad. Sci. U.S.A. 81*, 5685−5689.
33. Huang, G. S., and Oas, T. G. (1995) Submillisecond Folding of Monomeric λ Repressor, *Proc. Natl. Acad. Sci. U.S.A. 92*, 6878−6882.
34. Lacroix, E., Viguera, A. R., and Serrano, L. (1998) Elucidating the folding problem of alpha-helices: Local motifs, long-range electrostatics, ionic-strength dependence and prediction of NMR parameters, *J. Mol. Biol. 284*, 173−191.
35. Yang, W. Y., and Gruebele, M. (2003) Folding at the speed limit, *Nature 423*, 193−197.
36. Ballew, R. M., Sabelko, J., Reiner, C., and Gruebele, M. (1996) A single-sweep, nanosecond time resolution laser temperature-jump apparatus, *Rev. Sci. Instrum. 67*, 3694−3699.
37. Ozkan, S. B., Dill, K. A., and Bahar, I. (2002) Fast-folding protein kinetics, hidden intermediates, and the sequential stabilization model, *Protein Sci. 11*, 1958−1970.
38. Ervin, J., and Gruebele, M. (2002) Quantifying protein folding transition states with Phi-T, *J. Biol. Phys. 28*, 115−128.
39. Tanford, C. (1970) Protein Denaturation, *Adv. Protein Chem. 24*, 1−95.
40. Yang, W. Y., Pitera, J., Swopes, W., and Gruebele, M. (2004) Heterogeneous folding of the trpzip hairpin: full atom simulation and experiment, *J. Mol. Biol. 336*, 241−251.
41. Wolde, P. R. t., and Chandler, D. (2002) Drying-induced hydrophobic polymer collapse, *J. Mol. Biol. 311*, 373−393.
42. Sadqi, M., Lapidus, L. J., and Muñoz, V. (2003) How fast is protein hydrophobic collapse, *Proc. Natl. Acad. Sci. U.S.A. 100*, 12117−12122.
43. Burton, R. E., Myers, J. K., and Oas, T. G. (1998) Protein Folding Dynamics: Quantitative Comparison between Theory and Experiment, *Biochemistry 37*, 5337−5343.
44. Tanford, C. (1968) Protein Denaturation, *Adv. Protein Chem. 23*, 121−282.
45. Oliveberg, M., Tan, Y.-J., Silow, M., and Fersht, A. R. (1998) The changing nature of the protein folding transition state: implications for the shape of the free energy profile for folding, *J. Mol. Biol. 277*, 933−943.
46. Burton, R. E., Huang, G. S., Daugherty, M. A., Fullbright, P. W., and Oas, T. G. (1996) Microsecond Protein Folding Through a Compact Transition State, *J. Mol. Biol. 263*, 311−322.
47. Huang, D. M., and Chandler, D. (2000) Temperature and length scale dependence of hydrophobic effects and their possible implications for protein folding, *Proc. Natl. Acad. Sci. U.S.A. 97*, 8324−8327.
48. Matouschek, A., Otzen, D. E., Itzhaki, L. S., Jackson, S. E., and Fersht, A. R. (1995) Movement of the position of the transition state in protein folding, *Biochemistry 34*, 13656−13662.
49. Israelachvili, J. N. (1992) *Intermolecular and surface forces: with applications to colloidal and biological systems*, Academic Press, New York.
50. Ma, H., and Gruebele, M. (2004) *Proc. Natl. Acad. Sci. U.S.A.*, submitted for publication.
51. Zwanzig, R. (1988) Diffusion in a rough potential, *Proc. Natl. Acad. Sci. U.S.A. 85*, 2029−2030.
52. Nymeyer, H., García, A. E., and Onuchic, J. N. (1998) Folding Funnels and Frustration in Off-Lattice minimalist Protein Landscapes, *Proc. Natl. Acad. Sci. U.S.A. 95*, 5921−5928.
53. Skorobogatiy, M., Guo, H., and Zuckerman, M. (1998) Non-Arrhenius modes in the relaxation of model proteins, *J. Chem. Phys. 109*, 2528−2535.
54. Metzler, R., Klafter, J., Jortner, J., and Volk, M. (1998) Multiple Time Scales for Dispersive Kinetics in Early Events of Peptide Folding, *Chem. Phys. Lett. 293*, 477−484.
55. Yang, W. Y., and Gruebele, M. (2004) Detection-dependent folding kinetics as a probe of folding landscape microstructure, *J. Am. Chem. Soc. 126*, 7758−7759.
56. Becker, O. M., and Karplus, M. (1997) The topology of multidimensional potential energy surfaces: Theory and application to peptide structure and kinetics, *J. Chem. Phys. 22*, 1495−1517.
57. Mortenson, P. N., and Wales, D. J. (2001) Energy landscapes, global optimization and dynamics of the polyalanine Ac(ala)(8)-NHMe, *J. Chem. Phys. 114*, 6443−6454.

BI049113B